Enhanced absorption with multiple quadratically tapered elastic wedges of different lengths terminating a uniform beam

Angelis Karlos[a,*], Kristian Hook[b], Jordan Cheer[b]

[a]*Department of Robotics and Mechatronics, AGH University of Science and Technology, Al. A. Mickiewicza 30, Krakow, 30-059, Poland*
[b]*Institute of Sound and Vibration Research, University of Southampton, Highfield, Southampton, SO17 1BJ, United Kingdom*

Abstract

Tapered elastic wedges can be used to control flexural vibrations and this article explores a method of enhancing the performance of such terminations using multiple wedges. A system design where a uniform beam is terminated by multiple quadratically tapered wedges of different lengths is proposed, aiming to enhance the absorption of flexural vibrations. An analytical method based on the exact solution of the non-uniform one-dimensional Euler-Bernoulli beam is used to analyse this system, with the additional assumptions that the moments and forces at the junction from the side of the beam are balanced by the sums of the moments and forces of the wedges. The analytical model is compared with Finite Element simulations and its range of validity is discussed. Differences arise between the analytical and numerical results due to torsional effects, however, it is shown that a trident-shaped configuration can be used to suppress the effect of torsion. Simulations using the analytical model show that for the proposed multiple-wedge termination, more frequency bands of very low reflection, and thus very high absorption, appear compared to single-wedge terminations. Such bands of low reflection also occur at lower frequencies, where the absorptive capability of a single wedge is limited. An analysis of the zeros of the reflection coefficient in the complex-frequency plane is used to investigate the enhanced absorption through the concept of critical coupling. This analysis shows that the multiple-wedge termination leads to richer modal content due to the modal coupling between the wedges of different lengths, and that for appropriate length combinations very little damping can give very high absorption at certain frequencies. The proposed design thus provides significant enhancement of absorptive behaviour compared to a single-wedge termination.

Keywords: Elastic wedge, Acoustic Black Hole, multiple-wedge termination, enhanced absorption, analytical model

1. Introduction

The 'Acoustic Black Hole' (ABH) effect entails that flexural waves travelling along a one-dimensional wedge-like plate or beam with a power-law taper, of order greater than or equal to two, are theoretically completely absorbed close to the free tip, provided that the plate tapers down to zero thickness [1]. In practice, the tip will inevitably have a small non-zero thickness due to physical restrictions, which will lead to significant reflection from the truncated

*Corresponding author. E-mail address: angelis.karlos@agh.edu.pl

tip, thus greatly limiting the ABH effect. However, the addition of a thin viscoelastic layer on the truncated wedge will significantly enhance its absorptive behaviour, thus facilitating the applicability of the ABH effect for efficient vibration reduction [2, 3]. Research on the subject has expanded greatly in recent years, as has been reviewed in [4].

Two of the main challenges associated with improving the performance of ABHs are the extension of the vibration absorption efficiency to lower frequencies, and broadening or increasing the spectral density of the bands of low reflection. Several approaches have been presented in the literature for enhancing the absorbing performance of ABH terminations. Alternative thickness profiles to the standard power-law taper were analysed in [5], and an ABH thickness profile which involves a constant thickness added to a power-law taper, as well as including an extended platform termination, were investigated in [6], providing enhanced absorption, also at lower frequencies, compared with the standard power-law taper. An optimised thickness profile of a circular indentation on a plate, providing significant reduction of the plate vibration, was proposed in [7], which could also be utilised for beam terminations rather than plate indentations. Geometrical variations of the termination power-law taper were considered in [8], focusing on configurations that could benefit from additive manufacturing technologies. In [9], the distribution of the damping layer thickness along the wedge and the use of an added mass at the wedge tip were explored and shown to provide further potential for improved vibration control if properly tuned. A spiraling power-law termination was proposed in [10, 11], which allows a longer wedge to be confined to a small space and thus facilitates low-frequency absorption. Other techniques for enhancing the absorbing performance of the ABH termination that have been explored in the literature include the use of piezoelectric patches instead of damping layers [12], a vibro-impact ABH involving contact points that induce nonlinear waves, thus transferring energy from lower to higher frequencies and improving the low-frequency performance [13], and having imperfections in the termination tip [14, 15]. Another novel development was presented in [16], where a resonant beam damper with an ABH termination was proposed, which was designed to be attached to a vibrating system and thus avoid the need for modifications to the underlying structure to directly incorporate ABH design features. The use of multiple such dampers at different positions on the vibrating structure was also proposed, in order to efficiently suppress multiple resonances and increase the effective bandwidth. A different design for such an attachable vibration absorbing component was proposed in [17] based on a planar swirl-shaped ABH, which also induces torsional waves and achieves multi-directional vibration absorption.

Although systems with multiple ABH indentations in beams and plates have been explored, as reviewed in [4], only a single wedge has been considered in the literature for the case of beam terminations. This article explores a new geometrical configuration that consists of a multiple-wedge beam termination, where the wedges have different lengths. The motivation here derives from the fact that wedges of different lengths will resonate at different frequencies, and the multiple-wedge termination is thus expected to give richer modal content and result in an increase in the number of bands of low reflection. An analytical method based on the exact solution of the wave equation [18] is used to calculate the reflection coefficient for the multiple-wedge termination and provide physical insight into its characteristic behaviour. The analytical results are compared with those from Finite Element (FE) simulations, thus validating the general applicability of the analytical method, although its limitations are also illustrated. In particular, these limitations help to motivate a symmetric multiple-wedge geometry, which practically diminishes the effect of torsion for relatively narrow beams. The presented simulation results predict that the interaction between the wedges

generally leads to an enhancement in the absorption performance of the termination compared to a single-wedge termination, with more bands of low reflection, as well as bands of low reflection occurring at lower frequencies.

The remainder of this paper is organised as follows: In Section 2, the analytical model for a beam terminated by multiple wedges is presented and validated by comparing analytical results with those from FE models. The advantages of the multiple-wedge configuration compared to the single-wedge termination are discussed in Section 3. These are also illustrated through an analysis of the zeros of the reflection coefficient in the complex-frequency plane in relation to the critical coupling between the energy leakage and the damping. Conclusions are drawn in Section 4.

2. Modelling of a beam terminated by multiple quadratic wedges

2.1. Tapered-wedge model

In order to investigate the performance of a multiple-wedge beam termination, such as the one shown in Fig. 1 for the simplest case of two wedges, an analytical model for calculating the reflection coefficient from such a beam termination is first presented. This model is based on the exact solution of the non-uniform Euler-Bernoulli beam equation, which has previously been used for single-wedge terminations [18]. The wave equation for the complex amplitude $w(x, \omega)$ of the harmonic deflection of a non-uniform Euler-Bernoulli beam at angular frequency ω, after excluding the time-varying term $e^{i\omega t}$, is written as [18]

$$\left[EI(x)w''(x,\omega)\right]'' - \rho\omega^2 S(x)w(x,\omega) = 0, \tag{1}$$

where E and ρ are the Young's modulus and the density of the material, $I(x)$ is the second moment of area, $S(x)$ is the cross-sectional area, and the primes denote differentiation with respect to x. For a beam with a rectangular cross section with constant width b and varying thickness $h(x)$, the second moment of area and the cross-sectional area are given by $I(x) = bh^3(x)/12$ and $S(x) = bh(x)$. Losses in the model are included using a complex Young's modulus as $E = E_0(1 + i\eta)$, where E_0 and η are the lossless Young's modulus and the loss factor of the material, respectively. In the following, the uniform beam is considered to be lossless. The wedge-shaped terminations considered in this analysis have a quadratically varying thickness which can be expressed as

$$h(x) = h_0 \left(1 - \frac{x}{x_0}\right)^2, \tag{2}$$

where h_0 is the thickness at the junction with the uniform beam at $x = 0$, and x_0 is the length of the wedge when it is ideally tapered down to zero thickness. In practice, the wedge will have a non-zero thickness, h_t, at its tip, so that a wedge truncated at a length $l < x_0$ is considered, related to the length of the ideal taper by $l = \left(1 - \sqrt{H}\right) x_0$, where $H = h_t/h_0 < 1$ is the ratio of the thickness at the truncated tip to that at the junction.

The frequency dependence of the solutions to the wave equation in [18] is such that if the material parameters and the thickness of the junction and tip are kept unaltered, then keeping the quantity ωl^2 constant preserves the solutions. Therefore, for a single-wedge termination, changing the wedge length from l to l_s will produce a reflection coefficient that coincides with that of the former length when the frequency is shifted by $(l/l_s)^2$. The modulus of the reflection

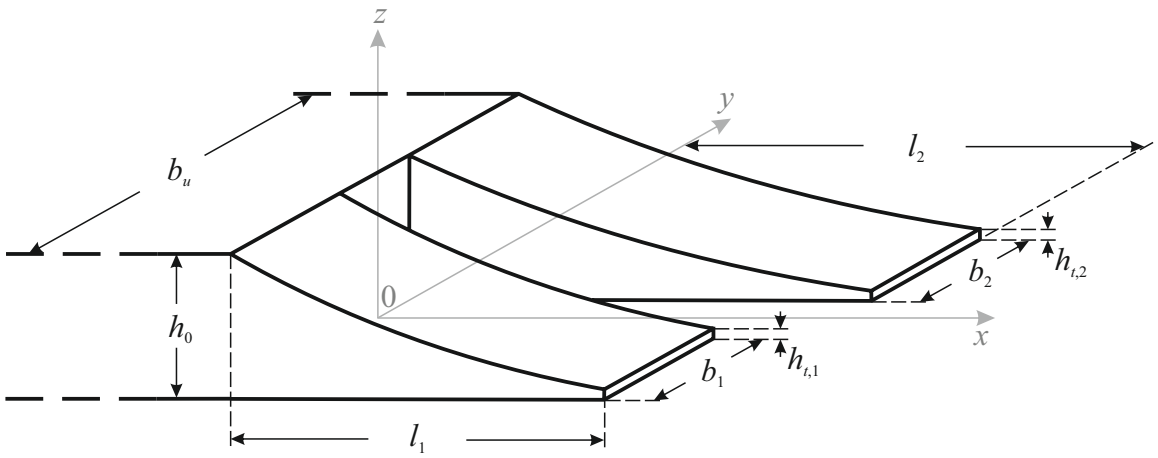

Figure 1. Schematic of a uniform beam terminated by two quadratic elastic wedges of different lengths.

coefficients of two quadratic wedges with the properties given in Table 1 is plotted in Fig. 2, calculated following the analysis in [18], where the two wedges have the same junction and truncation thickness but different lengths. In this logarithmic-frequency plot, the shift in the reflection coefficient caused by the change in length preserves its form, since the multiplication of the frequency by the factor $(l/l_s)^2$ accounts for addition on the logarithmic scale. Therefore, the logarithmic-frequency response can be continuously shifted by shifting the wedge length. The cut-on frequencies of the wedge terminations are also plotted, calculated as in [11], which also shift to a lower frequency with increasing length, as is well known.

Geometrical property	Value	Material property	Value
Junction thickness (h_0)	1 cm	Young's modulus (E_0)	68.9 GPa
Tip thickness (h_t)	0.5 mm	Density (ρ)	2700 kg·m^{-3}
Wedge length (l)	7 cm / 9 cm	Loss factor (η)	0.2

Table 1. Geometrical and material properties of the elastic wedge. The input beam is considered to be lossless.

It should be noted that in this analysis, the effect of adding a damping layer to the wedge is modelled phenomenologically, by employing a large uniform damping factor for the material. This approach is imposed by a limitation of the analytical model. Therefore, even though the values of the Young's modulus and the density given in Table 1 are those of aluminium, the values of the damping factor used in much of this analysis are significantly larger than those of aluminium or its alloys, but are instead consistent with the thin damping layers that would in practice be applied to the wedge.

2.2. Reflection coefficient of multiple-wedge termination

As observed above, as the length of a single wedge termination is changed, the frequencies over which the bands of low reflection occur are shifted and this motivates the idea of exploring the design of a termination with multiple quadratic wedges of different lengths. Such a system is expected to have richer modal content, due to the structural modes of the wedges occurring at different frequencies. A particular design with two wedges is first presented,

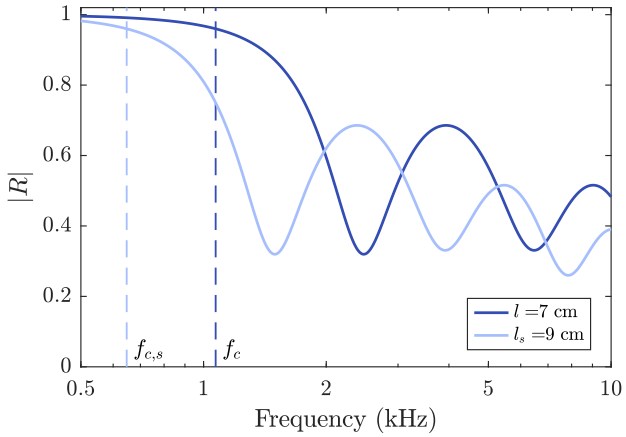

Figure 2. Modulus of the reflection coefficient of two truncated quadratic wedges of the same truncation thickness, but different lengths. The corresponding cut-on frequencies are also shown. The two reflection coefficients coincide if either is shifted in frequency by the square of their lengths' ratio.

as shown in Fig. 1, but designs that incorporate additional terminating wedges can also be modelled by the same method. The vibrational response of this system can be modelled analytically by making the assumption that the wave in the uniform beam can be regarded as the superposition of only three wave components, as in the single-wedge termination reported in [18]. These are the incident wave, the reflected travelling wave and the reflected evanescent wave. The underlying assumption with this approach is that the uniform beam vibrates uniformly across its width in the y direction, even at the junction where the two different-length wedge terminations will vibrate both in and out of phase with each other depending on the frequency and the tuning of the wedge lengths. This assumption means that any torsion introduced by the asymmetrical termination geometry will be neglected in the analytical model; the influence of this on the accuracy of the model will be explored further in Section 2.3 via an FE model. An alternative configuration with three wedges arranged symmetrically is then proposed, which physically suppresses torsion.

The reflection coefficient for a beam terminated by tapered wedges can be calculated by solving the system of equations that express the boundary conditions. To this end, the travelling and evanescent waves in the uniform beam and in each wedge have to be formulated. A unit input amplitude for the incident wave is assumed for convenience, which, due to the assumed linearity of the system, will not affect the reflection and transmission coefficients. The reflective behaviour of the system is represented by the total reflection coefficient, or simply the reflection coefficient henceforth, which is defined as

$$R = \frac{w_r(0)}{w_i(0)}, \tag{3}$$

where w_i is the incident wave from the uniform beam, w_r is the reflected travelling wave in the uniform beam, (0) denotes that these values are evaluated at $x = 0$ and the notation indicating the frequency dependence is omitted for compactness. The wave in the uniform beam is expressed with respect to reflection coefficients as

$$w_u = \mathrm{e}^{-\mathrm{i}k_u x} + R\mathrm{e}^{\mathrm{i}k_u x} + R_e\mathrm{e}^{k_u x}, \tag{4}$$

where R_e is a reflection coefficient relating the amplitude of the reflected evanescent wave to the incident wave, and k_u is the beam wavenumber, which for a uniform lossless beam of thickness h_0 is given by $k_u = \sqrt[4]{12\rho\omega^2/E_0h_0^2}$ [19]. The wave in each of the wedges, j, is written as [18]

$$w_{w,j} = \left(1 - \frac{x}{x_{0,j}}\right)^{-3/2} \left[\left(1 - \frac{x}{x_{0,j}}\right)^{\mathrm{i}\kappa_j} T_j + \left(1 - \frac{x}{x_{0,j}}\right)^{-\mathrm{i}\kappa_j} R_{w,j} + \left(1 - \frac{x}{x_{0,j}}\right)^{\alpha_j} T_{e,j} + \left(1 - \frac{x}{x_{0,j}}\right)^{-\alpha_j} R_{we,j}\right], \quad (5)$$

where

$$\kappa_j = \frac{1}{2}\sqrt{-17 + 8\sqrt{1+\psi_j}}, \quad \alpha_j = \frac{1}{2}\sqrt{17 + 8\sqrt{1+\psi_j}} \quad (6)$$

are the propagation and decay coefficients, respectively, where $\psi_j = 3\rho\omega^2 x_{0,j}^4/E_j h_0^2$, and appropriate reflection and transmission coefficients have been defined. In the following, wedges with the same loss factor at a given configuration are considered, so that E_j is the same for different j.

Following the assumption that the uniform beam vibrates uniformly across its width, there are $4n + 2$ boundary and continuity conditions, where n is the number of wedges. These are two free-end conditions at each of the wedge tips, expressed as

$$w''_{w,j}(l_j) = 0, \; w'''_{w,j}(l_j) = 0, \quad (7)$$

two continuity conditions for the displacement and slope of each of the wedges with the uniform beam, expressed as

$$w_u(0) = w_{w,j}(0), \; w'_u(0) = w'_{w,j}(0), \quad (8)$$

and two equilibrium conditions at the junction, one for the bending moment and one for the shear force, expressed as

$$B_u(0)w''_u(0) = B_{w,1}(0)w''_{w,1}(0) + B_{w,2}(0)w''_{w,2}(0) \quad (9)$$

and

$$B_u(0)w'''_u(0) = B'_{w,1}(0)w''_{w,1}(0) + B_{w,1}(0)w'''_{w,1}(0) + B'_{w,2}(0)w''_{w,2}(0) + B_{w,2}(0)w'''_{w,2}(0), \quad (10)$$

where $B_u = E_u b_u h_0^3/12$ is the bending stiffness of the uniform beam and $B_j = E_j b_j h_j^3/12$ is the bending stiffness in each of the wedges. In the equilibrium conditions, the bending moment and the shear force from the uniform side are balanced by the sum of the corresponding quantities for the two wedges. Calculating the derivatives of Eqs. (4) and (5) and substituting these into the boundary conditions given by Eqs. (7), (8), (9) and (10) gives a $(4n+2)\times(4n+2)$ system of equations. Solving this system provides the reflection coefficient defined by Eq. (3). In the following analysis, a beam terminated by two wedges is considered, which requires the solution of a 10×10 system of equations.

2.3. FE modelling

In this section, a 3D FE model of a beam with a double-wedge termination is presented and this will be used in Section 2.4 to validate and demonstrate the limitations of the analytical double-wedge model. The FE model has been implemented using the Solid Mechanics Physics Module in COMSOL Multiphysics. The termination has been

implemented using the dimensions detailed in Table 1 and each wedge uses the same quadratic power-law profile described for the analytical model.

In order to enable a comparison between the analytical model and the FE model results, the reflection coefficient has been calculated from the FE model by exciting the beam with an evenly distributed force at its uniform end and using the two sensor wave decomposition approach described in [20, 21, 22]. The wave decomposition method has a low frequency limit that depends on the evanescent wave components having sufficiently decayed at the measurement locations and a high frequency limit that depends on the spatial aliasing limit imposed by the spacing between the two sensors. In the presented FE study, to accommodate for a 100 Hz – 10 kHz frequency range, the beam was set to be 75 cm long and the sensor array was located 36.5 cm from the excitation force and 36.5 cm from the taper junction, with a spacing of 2 cm between the sensors. These values were selected by following the expressions describing the limits in [22]. In order to determine the meshing resolution required to accurately model the beam with the double-wedge termination, a convergence study has been performed. Swept, triangular elements have been used to mesh the beam and wedges and the resolution has been varied between 0.2 and 7 elements per wavelength. For each mesh, the reflection coefficient has been calculated at the highest frequency of interest (10 kHz), which will require the finest mesh. From this study it was determined that a mesh resolution greater than four elements per wavelength was suitable. Therefore, a minimum of four elements per wavelength have been used in the FE model results presented in the following section.

2.4. Validation and limitations of the analytical double-wedge model

In order to validate the analytical model for the double-wedge termination, and examine its limitations, a comparison between the analytical and FE model results is carried out in this section. In the double-wedge termination, torsion is expected to occur around the beam axis, due to the different lengths of the two wedges and their resulting responses. However, torsion is not accounted for by the analytical model, since the wave equation considered is one-dimensional. A comparison between the reflection coefficients calculated using either the FE model or the analytical model for a beam with two wedge terminations of lengths 7 and 9 cm and a loss factor $\eta = 0.2$ is shown in Fig. 3a for two different beam widths. In each FE model, the width of the two wedges is equal to 47.5% of the beam width, leaving a gap of 5% between the wedges along the y-axis. The analytical model is invariant to scaling along the y-axis, so that the analytical results in Fig. 3a are the same for both widths.

From the results presented in Fig. 3a it can be seen that for the narrower, 1 cm beam width the analytical and FE results are quite consistent. However, relatively significant differences occur between the analytical and FE results for the wider, 4 cm beam width. In particular, it can be seen that fluctuations occur in the FE results, which are due to the torsional effects that are neglected in the analytical model. These fluctuations are less pronounced for the narrower beam since it is more rigid with respect to torsional excitation. It should be noted that the effect of torsion also depends on the length of the uniform beam, with longer beams resulting in a larger spectral density of torsional modes. Shorter beams, therefore, will be less affected by torsion and thus more accurately represented by the analytical model.

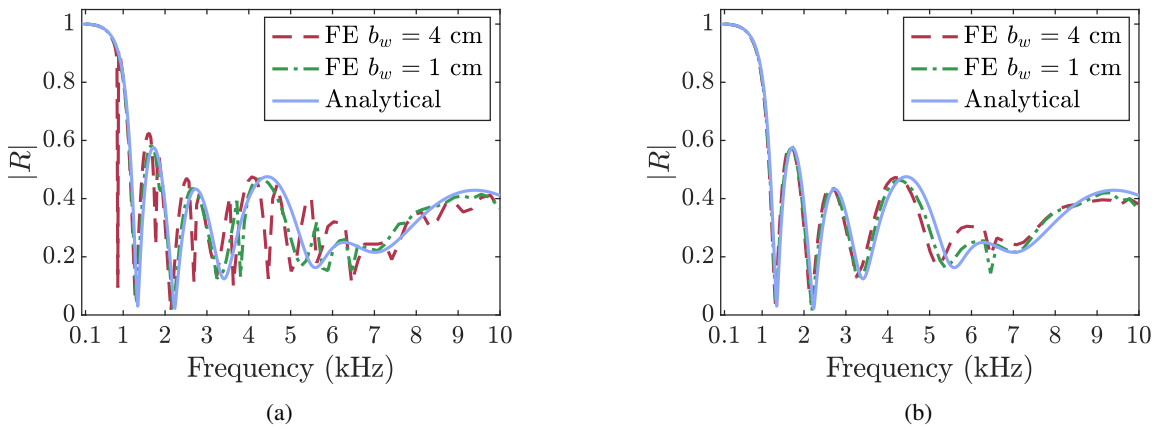

Figure 3. Modulus of the reflection coefficient of a uniform beam terminated by (a) two truncated quadratic wedges of the same truncation thickness and different lengths $l_1 = 7$ cm and $l_2 = 9$ cm, (b) three truncated quadratic wedges in a symmetric trident-shaped configuration, calculated either with FE models of different beam widths or with the analytical model. In (b), the length of the two outer wedges is $l_1 = 7$ cm and the length of the middle wedge is $l_2 = 9$ cm. The analytical model is invariant to scaling along the width, so that the presented results are the same for either beam width.

2.5. Symmetric three-wedge configuration that suppresses torsion

In practice, it may not be possible to reduce torsion by decreasing the length of the beam, however, torsion can be considerably suppressed by using a symmetric system with respect to the $x - z$ plane. This can be realised by using an alternative three-wedge design, as shown in Fig. 4, where the two wedges on the sides are identical and the one in the middle has a different length. The analytical model presented here for the two-wedge termination can be used to simulate this symmetric configuration, provided that the two identical wedges on the sides are treated as a single wedge whose width is the sum of their widths.

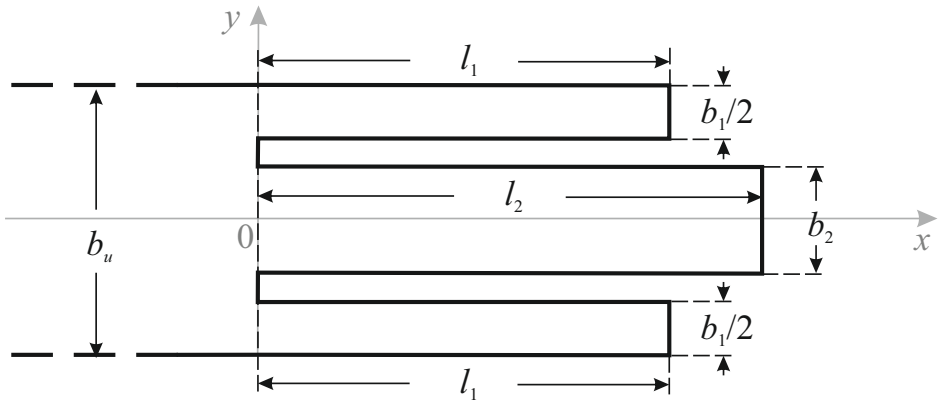

Figure 4. Top-view schematic of a symmetric configuration of a uniform beam terminated by three quadratic elastic wedges, where the two outer ones are identical.

The reflection coefficients for the trident-shaped configuration shown in Fig. 4, calculated using the analytical model and FE models for two different beam widths, are shown in Fig. 3b. From these results it can be seen that the additional fluctuations due to torsion observed in Fig. 3a are absent here, which shows that the symmetric design

effectively suppresses torsion. Consequently, it can also be seen that the reflection coefficient calculated with the analytical model matches the results from the FE models quite accurately, especially for the narrower beam. Some discrepancy is observable, although this is very small up to about 4.5 kHz for the geometrical and material properties used here. Larger discrepancies are observed between the analytical results and the FE results for the wider beam, although these are still not significant up to about 4.5 kHz. The better correspondence between the analytical results and the FE results for the narrow beam is again related to the assumption that the response across the width of the beam is constant in the analytical model, which is closer to being physically satisfied in the case of the narrow beam. Overall, the analytical model predicts the flexural behaviour of the symmetric triple-wedge termination well, albeit with an increasing deviation at higher frequencies. Nevertheless, it serves well as a very fast modelling tool both for general analysis and design purposes.

3. Investigation of the multiple-wedge termination response

3.1. Dependence of the reflection coefficient on the wedge lengths

In this section, an investigation into the design and performance of the multiple-wedge termination is presented. In particular, it is investigated how the lengths of the multiple wedges should be tuned to maximise performance. It was demonstrated above that the analytical model better predicts the reflection from a symmetric trident-shaped termination, but also predicts the reflection from a double-wedge termination with reasonable accuracy provided that the beam is relatively narrow. Since the analytical model is the same for the double-wedge and the symmetric trident-shaped configurations, the results presented below may in principle correspond to either design, albeit with greater accuracy for the latter. For ease of reference, these two designs will be referred to collectively as a multiple-wedge termination in the following analysis, in contrast to the single-wedge termination.

In the first instance, the modulus of the reflection coefficient of the beam terminated by a multiple-wedge configuration with wedge lengths of 7 and 9 cm is plotted in Fig. 5, along with the corresponding reflection coefficients for the single-wedge terminations. From these results it can be seen that the system with the multiple-wedge termination presents some very narrow frequency bands of low reflection, contrary to the single-wedge configurations, whose reflection coefficients only present relatively ‘shallow’ fluctuations with frequency. In particular, at lower frequencies, nearly zero reflection occurs at around 1.3 kHz and 2.2 kHz for the multiple-wedge system properties considered here, which corresponds to a nearly perfectly absorbing termination. These results show that combining two wedges of different lengths not only increases the number of bands of low reflection, but also reduces the general level of reflection over frequency.

To illustrate the effect of different length combinations on the reflective behaviour of the multiple-wedge termination, a set of contour plots is presented in Fig. 6. In the upper graphs, Figs. 6a and 6b, the modulus of the reflection coefficient for a single wedge termination is plotted as a function of frequency and wedge length, whereas the lower graphs, Figs. 6c and 6d, correspond to multiple-wedge terminations where the length l_1 is fixed at 7 cm and the length l_2 is varied. The graphs on the left correspond to a loss factor of $\eta = 0.02$ whereas the graphs on the right are for a larger loss factor of $\eta = 0.2$. The curve at low frequencies, which is the same for all graphs, corresponds to the cut-on frequency of the wedge whose length is being varied in each case.

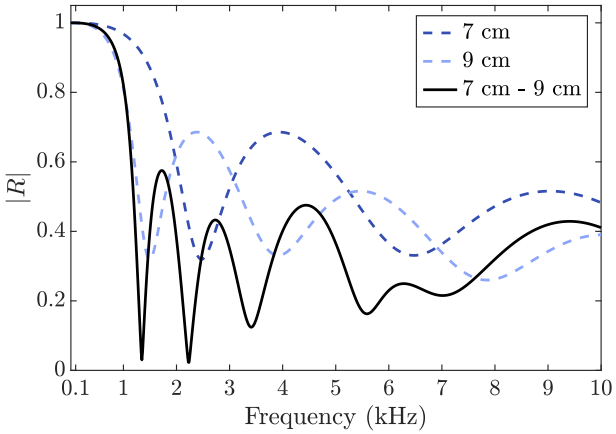

Figure 5. Modulus of the reflection coefficient of a uniform beam with a multiple-wedge termination, with two quadratic wedges of the same truncation thickness but different lengths $l_1 = 7$ cm and $l_2 = 9$ cm. The moduli of the reflection coefficients for beams terminated by a single-wedge of the same width as the beam and lengths of 7 or 9 cm are also plotted.

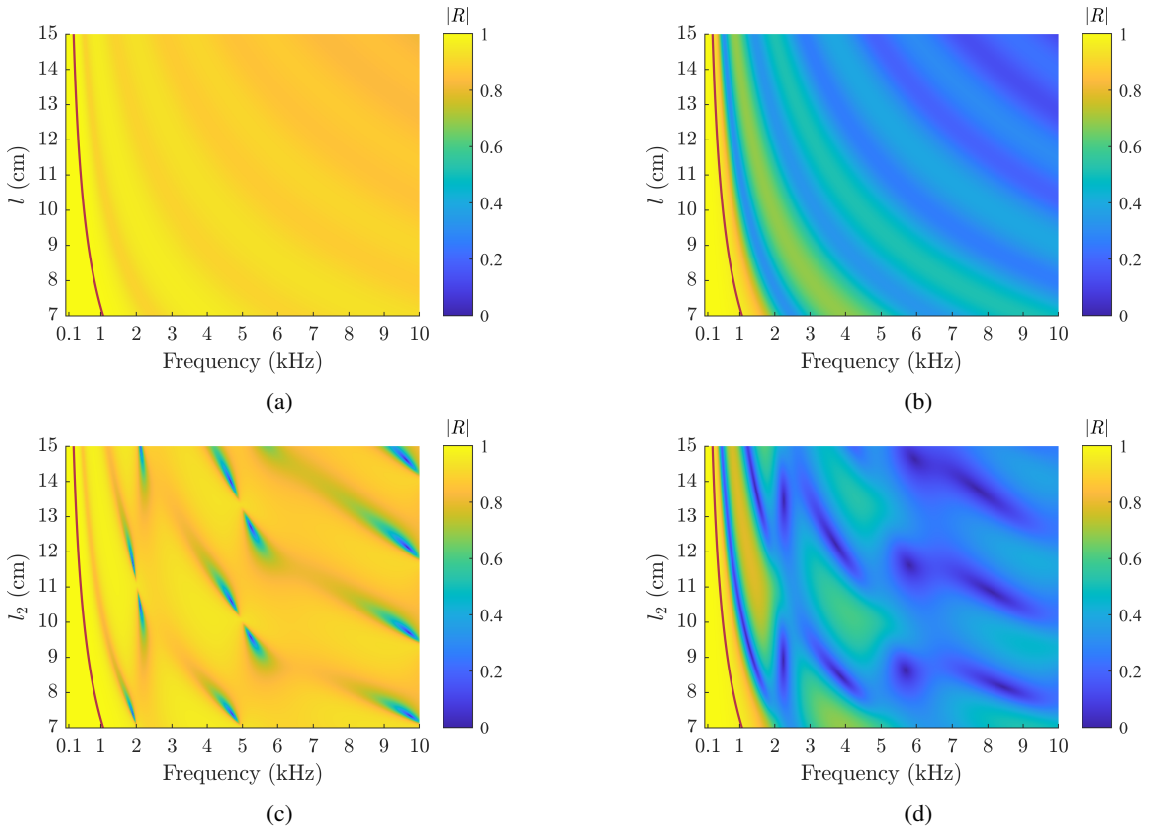

Figure 6. Contour plots of the modulus of the reflection coefficient for a single-wedge termination against frequency and against the wedge length for (a) $\eta = 0.02$ and (b) $\eta = 0.2$. Contour plots of the modulus of the reflection coefficient for a multiple-wedge termination with $l_1 = 7$ cm against frequency and against the length l_2, for (c) $\eta = 0.02$ and (d) $\eta = 0.2$. In all plots, the curve indicates the cut-on frequency, which for the multiple-wedge termination coincides with the cut-on frequency of the l_2 wedge.

From comparing the two upper graphs in Fig. 6 it can be seen that the reflection coefficient decreases when increasing the damping in the single-wedge termination as expected and well-documented in the literature. It can also be seen from the two upper graphs that frequency bands corresponding to lower levels of reflection decrease in frequency as the length of the single wedge is increased, as is also well known. It is interesting, however, to observe the more complex behaviour that occurs with the multiple-wedge configurations, as shown in the lower graphs in Fig. 6. From these results it can be seen that, even in the case of low damping, the introduction of a second wedge of different length produces narrow bands of very low reflection, as can be seen by the regions of very small reflection coefficient in Fig. 6c compared to the relatively uniform high reflection seen in Fig. 6a. These regions of low reflection occur at different frequencies for different length combinations and they appear to follow a quasi-periodic pattern when varying the length of the second wedge, that is, along the vertical axis of the graph. It is noted that the two single-wedge reflection coefficients plotted in Fig. 5 correspond to the reflection coefficients along the horizontal lines at $l = 7$ cm and $l = 9$ cm in Fig. 6b, whereas the multiple-wedge plot in Fig. 5 corresponds to the reflection coefficient along the horizontal line at $l_2 = 9$ cm in Fig. 6d. Given the length of $l_1 = 7$ cm, the particular length of $l_2 = 9$ cm plotted in Fig. 5 was chosen by inspection of Fig. 6d to give regions of very low reflection at low frequencies, where the single-wedge termination is less effective. Regions of very low reflection at higher frequencies can be achieved by using different length combinations and the insight shown by the results presented in Fig. 6 can help the multiple-wedge designer select the appropriate combination of wedge lengths based on the control objective.

3.2. Critical coupling of energy leakage and damping

To provide further insight into the characteristic behaviour of the multiple-wedge termination, the absorptive behaviour can be analysed through the zeros of the reflection coefficient in the complex-frequency plane [23]. Such an approach was used for single-wedge ABH terminations to analyse the tunability of perfect absorption with a variation in the damping [9]. It was demonstrated in [23] for the case of Helmholtz resonators, and then in [9] for single-wedge ABH terminations, that in the absence of damping, the modulus of the reflection coefficient has a set of complex conjugate pairs of poles and zeros, which are thus arranged symmetrically in the complex-frequency plane with respect to the line of zero imaginary frequency (or real-frequency axis). The actual behaviour of the system corresponds to the response for purely real frequencies, which in the absence of damping gives total reflection from the termination. However, the imaginary parts of the poles express the energy leakage rate of the corresponding modes, where the leakage corresponds to the energy of the mode that is reflected from the wedge back to the input beam. Thus, perfect absorption for a given mode can be achieved by introducing the appropriate amount of damping which balances the leakage, a condition called critical coupling [23]. Poles and zeros with large-magnitude imaginary frequency correspond to large energy leakage, which therefore requires more damping to compensate, and accordingly, poles and zeros with small-magnitude imaginary frequency require little damping to achieve critical coupling.

A complex-frequency analysis of the reflection coefficient is considered here for various multiple-wedge configurations. A set of contour plots showing the modulus of the reflection coefficient in the complex-frequency plane are shown in Fig. 7 for $\eta = 0$. As in the case of a single-wedge termination [9], there is a number of complex conjugate pairs of poles and zeros. The focus, however, here is on the zeros, which appear in the negative-imaginary

frequency half-plane, since their upward shifting with damping will lead to critical coupling, as will be seen. Figure 7a shows the zeros of a single-wedge termination, from which it can be seen that only two zeros are present within the considered frequency range. It should be noted that the zero that is furthest from the real-frequency axis is broader, that is, the quality factor of the corresponding resonance is smaller, a condition which holds in general [23].

When moving to a multiple-wedge termination, the modes of vibration are now coupled due to the interaction between the wedges through the junction with the uniform beam. This coupling provides a new mechanism of absorption where, under certain conditions, the energy oscillates between the two wedges without flowing back to the beam, so that total absorption, that is, critical coupling, can be achieved with little damping, as will be illustrated in the following section. The trapping of the energy in the multiple-wedge termination leads to displacements of high amplitude at the wedge tips, as was verified by simulations not presented here, so that a small amount of damping is sufficient to dissipate the incident energy as heat. In contrast, in the case of a single-wedge termination, there is only one, bi-directional, path for the energy to flow, that is, between the beam and the wedge, so that, in low and medium frequencies, critical coupling can only be achieved with significant damping to compensate for the energy reflected at the truncation.

Figure 7b shows the reflection coefficient complex-frequency contour plot for the multiple-wedge termination where the length of the second wedge is greater than the first. This plot shows that, for the multiple-wedge termination with l_2 slightly larger than l_1, a number of additional zeros, and thus modes, appear at certain frequencies with small-magnitude imaginary parts, as indicated by the arrows, and are thus close to the real-frequency axis. These zeros with small-magnitude imaginary parts correspond to vibration modes where most of the energy oscillates between the wedge terminations and can thus be critically coupled with little damping, as will be illustrated in the following section. As the length l_2 increases, as in Figs. 7b to 7e, the new zeros shift towards lower frequencies, and they also shift towards larger-magnitude imaginary frequencies. This increases the low frequency performance of the multiple-wedge configuration, as shown by the reflection coefficient results presented in Fig. 6, but also means that a higher level of damping is required to obtain critical coupling. At the same time as the new zeros are shifted, the two zeros that were present in the single-wedge termination shift towards the real-frequency axis, which means that less damping is required to achieve critical coupling for these zeros. Further increasing l_2 can cause all of the zeros to be shifted both up and down in frequency, depending on the relative values of the two wedge lengths, as well as a further shift of the new zeros towards lower frequencies.

The zeros for a 9 cm long single-wedge termination are also shown in Fig. 7f. Comparing Fig. 7e for the multiple-wedge termination with $l_1 = 7$ cm and $l_2 = 9$ cm with the plots for the corresponding single-wedge terminations plots in Figs. 7a and 7f, it can be seen that the multiple-wedge termination has five zeros within the presented frequency range, which is the sum of the number of zeros present for the two single-wedge terminations. Therefore, the multiple-wedge termination can be considered as having a combined modal structure based on the corresponding structure of the two single-wedge terminations.

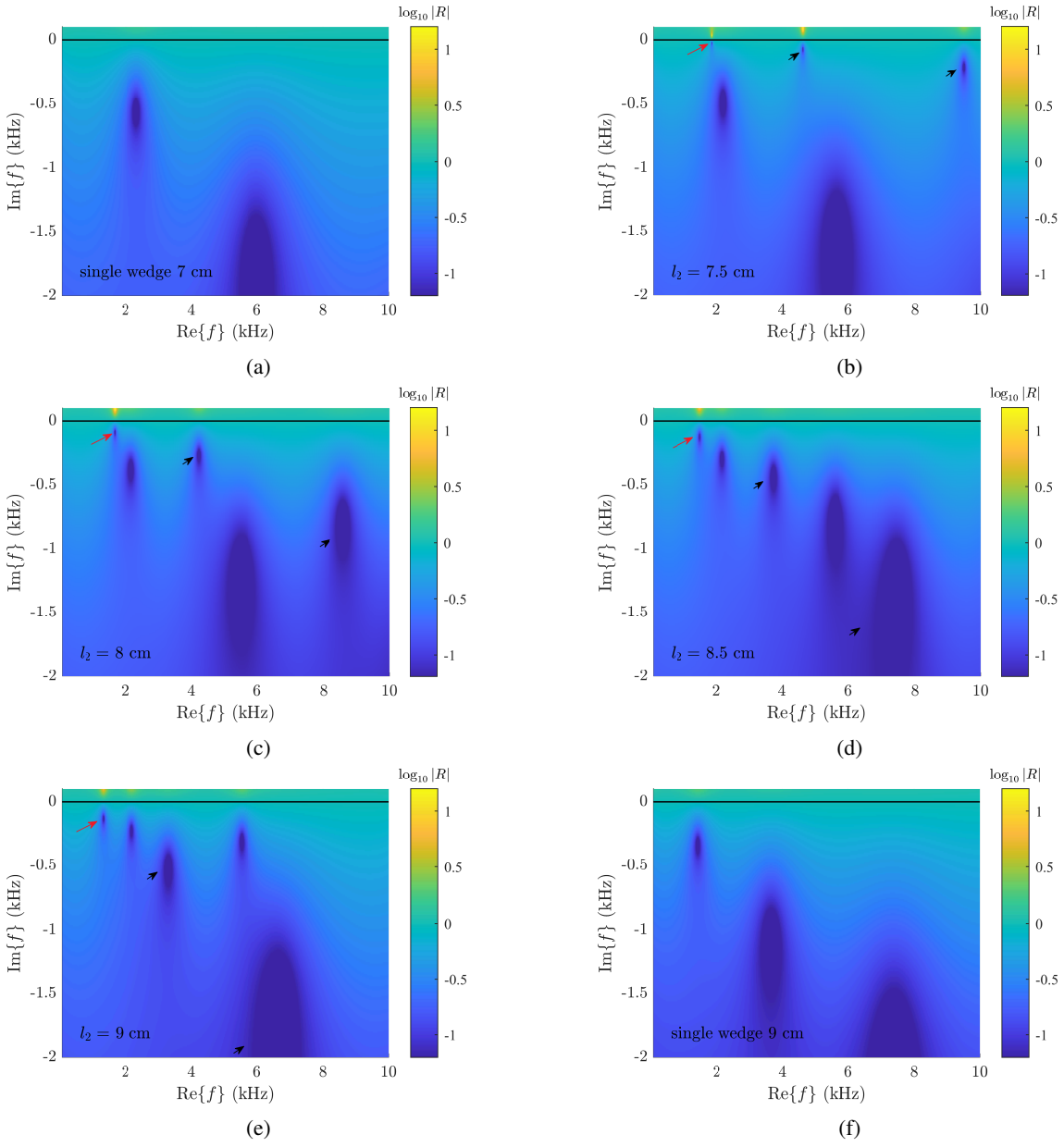

Figure 7. Logarithm of the reflection coefficient modulus in the complex frequency plane with $\eta = 0$ for (a) a single-wedge termination with $l = 7$ cm, (b)-(e) multiple-wedge terminations with $l_1 = 7$ cm and different l_2, (f) a single-wedge termination with $l = 9$ cm. Dark areas of low reflection appear around the zeros of the reflection coefficient. The arrows point to the areas around the additional zeros that appear when $l_2 > l_1$, with the coloured one pointing at the zero with the lowest real frequency.

3.3. Critical coupling with little damping

To further investigate the presence of the narrowband regions of very low levels of reflection for lightly damped multiple-wedge configurations, as previously noted in reference to Fig. 6c, the first zero that appears due to the difference of the wedge lengths, indicated by the coloured arrow in Figs. 7b to 7e, is shown in Figs. 8a and 8b in two instances for l_2 slightly larger than $l_1 = 7$ cm. The zero is seen to emerge almost on the real-frequency line, and is thus very narrow, for $l_2 \approx l_1$ in Fig. 8a, and then it shifts in real frequency, and it also shifts towards larger-magnitude imaginary frequencies and thus broadens when l_2 is increased in Fig. 8b. The fact that this zero has a very small imaginary part means that very little damping is required to critically couple the leakage of reflected energy. Introducing the appropriate damping will thus lead to zero reflection at the specific frequency. This is illustrated in Figs. 8c and 8d for the lengths used in Figs. 8a and 8b, respectively, where the critically coupled damping shifts the zeros to the real-frequency line. Figures 8a to 8d also illustrate that the zeros that appear for $\eta = 0$ retain their bandwidth when η is increased [23].

Plots of the reflection coefficients for the two cases of length combinations and damping presented in Figs. 8c and 8d are shown in Figs. 8e and 8f, which illustrate that the reflection coefficient vanishes at the frequency of the zero, whereas in the case of a single termination the reflection coefficient is practically unity throughout the considered frequency range. More low-reflection points also appear at higher frequencies. The former case, Fig. 8e, where the damping is of the order of the material's structural damping, demonstrates that the multiple-wedge termination can fully absorb certain frequencies even without the addition of damping layers, although the effect is very narrowband. The latter case, Fig. 8f, shows that the combination of slightly larger l_2 and damping broadens the range of low reflection, although this still remains narrow for such low amounts of losses. In both cases, it is the coupling of the leakage with the damping that results in low reflection, whereas higher damping will violate the critical coupling and thus deteriorate the effect. Plots for lengths of two different orders of rounded precision are also shown in the figures, showing that the critical coupling is sensitive to the length accuracy, although even millimetre precision retains a relatively good performance for the case of $\eta = 0.01$.

Since the modes of vibration in the multiple-wedge termination are coupled, total absorption corresponds to the wedges vibrating in a coupled way so that the incident energy is trapped and oscillates between them and is thus absorbed there, without being reflected back to the beam. In particular, the emergence of the new zeros close to the real-frequency axis with wedges of slightly different lengths illustrates that the coupling of the wedges through the boundary conditions at the junction is such that for given length combinations and at certain frequencies, total absorption is possible with very little damping. Simulations, not included here, showed that the zeros emerge even closer to the real-frequency line for $l_2 \approx l_1$ compared to Fig. 8a, albeit they are even narrower. The absorption mechanism due to the coupled modes is different from that in a single-wedge termination, where absorption can only occur due to the modes of the single wedge. The single-wedge modes are always relatively far from the real-frequency axis in the absence of damping, as can be seen in the corresponding straight lines in Fig. 9 analysed below, which means that the single-wedge termination always requires significant damping to give total absorption at a certain frequency. The mechanism of absorption through the coupled modes in the multiple-wedge termination thus provides a novel way of achieving total absorption with little damping.

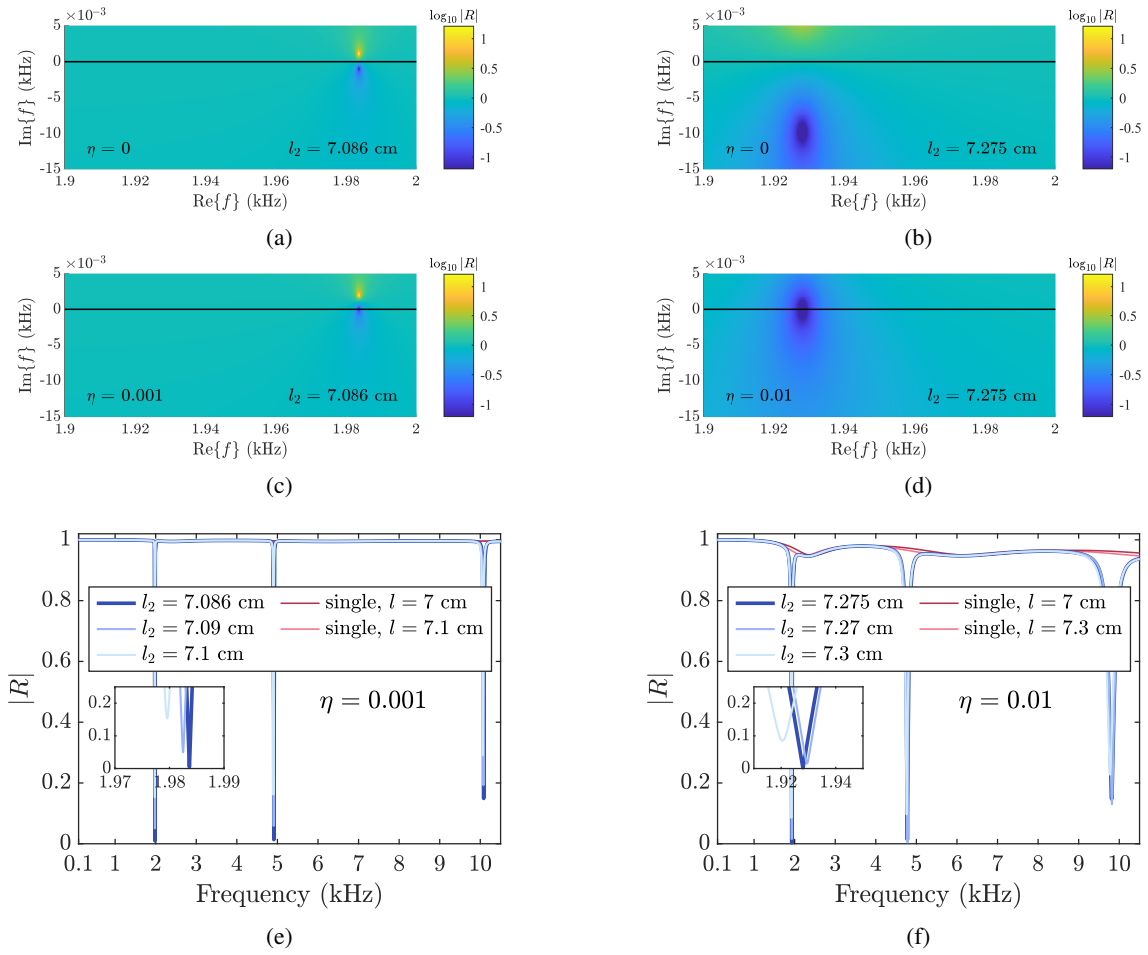

Figure 8. Logarithm of the reflection coefficient modulus in the complex frequency plane with (a) and (b) $\eta = 0$, (c) and (d) critically coupled η, for multiple-wedge terminations of different l_2 that are slightly larger than l_1. The dark areas of low reflection correspond to the zero of the reflection coefficient indicated by the coloured arrow in Figs. 7b to 7f. (e) and (f) Modulus of the reflection coefficient of a uniform beam terminated by quadratic wedges with $l_1 = 7$ cm and the second length adjusted and rounded at different orders of precision to give low reflection at a frequency around 2 kHz, with (e) $\eta = 0.001$, (f) $\eta = 0.01$. In (e), the modulus of the reflection coefficients for single-wedge terminations with $l = 7$ cm and $l = 7.1$ cm are also plotted, which both have values very close to 1 for such low damping and are practically indistinguishable from each other at the graph's scale. In (f), the reflection coefficients for single-wedge terminations with $l = 7$ cm and $l = 7.3$ cm are also plotted, which differ little from each other.

3.4. Movement of zeros in the complex-frequency plane with varying second wedge length and damping

To provide further insight into the design of multiple-wedge terminations, Fig. 9 shows a plot demonstrating how the first four zeros, starting from the lowest frequency zero, vary with increasing l_2 and for different values of damping in the complex-frequency plane. The first and third zeros correspond to the modes introduced by the second wedge and thus only appear for $l_2 \neq l_1$. It can be seen that for no damping, the zeros of these two modes originate very close to the real-frequency axis and, therefore, critical coupling requires very little damping in this case. The second and fourth zeros correspond to the l_1 wedge and, therefore, occur in the single-wedge termination as shown in Fig. 7a, and their starting points, corresponding to $l_2 = l_1 = 7$ cm, are noted with circles in Fig. 9. The movement of these zeros as the single-wedge length is increased from 7 to 14 cm is shown by the straight lines in Fig. 9. These trajectories show

that these zeros move towards lower frequencies and smaller absolute values of imaginary frequency. This variation shows that even though single-wedge terminations with longer wedges move the zeros towards lower frequencies, as is well known, they still require similar amounts of damping to give perfect absorption because damping shifts the zeros upwards by less at lower frequencies, as previously observed in [9]. Conversely, for the multiple-wedge termination, it can be seen that the movement of the second and fourth zeros is more complex, but they are always closer to the real-frequency axis than for the single-wedge configuration. This further illustrates the advantage of the multiple-wedge termination, where for given combinations of lengths the zeros move closer to the real-frequency axis, and thus require very little damping to achieve critical coupling.

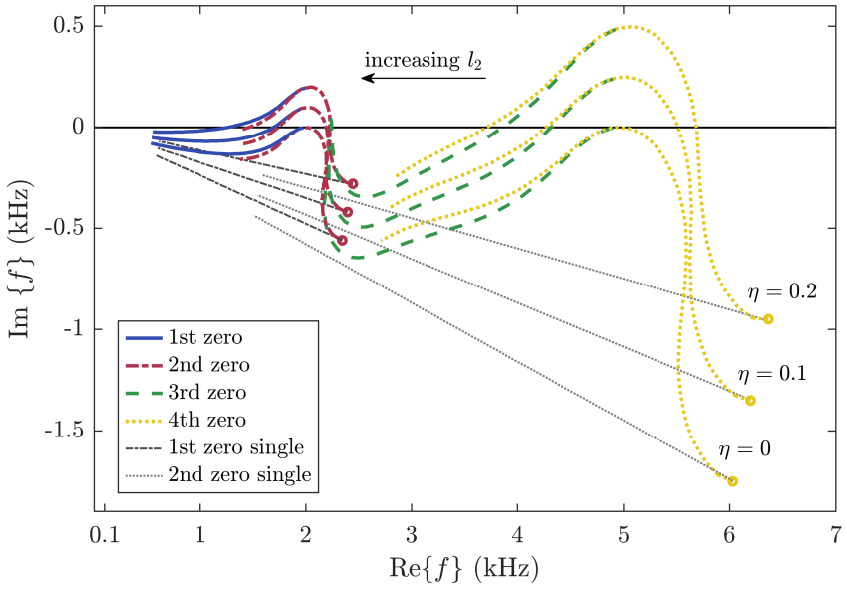

Figure 9. Shifting of the first four complex-frequency zeros of the reflection coefficient with increasing second-wedge length l_2 from 7 to 14 cm, for different values of η (from bottom to top, η =0, 0.1, 0.2). Increasing l_2 generally shifts the zeros towards lower frequencies. The circles indicate the starting points of the 2nd and 4th zero for a single-wedge termination with l = 7 cm, which, for η = 0, correspond to the two zeros shown in Fig. 7a. The straight lines follow the first two zeros of a single-wedge termination, which coincide with the second and fourth zeros of the multiple-wedge termination, as they shift towards lower frequencies when the length is varied from 7 cm to 14 cm.

For the first and third zeros, it can be seen from the results presented in Fig. 9 that increasing l_2 first shifts them away from the real-frequency axis, but beyond a certain value of l_2, they are shifted back towards the real-frequency axis, as can be more clearly seen for the third zero. For the second and fourth zeros the trend is opposite, first shifting upwards and then downwards in frequency. In general, the plot lines for a given zero and a certain value of η appear to approximately merge with those of the previous zero beyond some value of l_2, thus approximately forming a continuum. This means that as l_2 changes, and the new zeros introduced by the coupling of the wedges shift away from the real-frequency axis, as observed in Fig. 7, the new modes introduced by the multiple-wedge terminations shift to those present in the single-wedge termination and vice versa. Consequently, the second and fourth zeros for $\eta = 0$ in Fig. 9 also reach the real frequency axis for appropriate l_2, which in this case occurs for $l_2 \approx 11.05$ cm and $l_2 \approx 10.05$ cm for the respective zeros. Therefore, critical coupling with very little damping also occurs for length

combinations where l_1 and l_2 do not have similar values.

In terms of the influence of damping on the movement of the zeros, Figure 9 shows that increasing the damping generally shifts the zeros upwards in the complex-frequency plane in a continuous way, with those at higher frequencies being shifted more than those at lower frequencies, as was also observed for the single-wedge termination with added damping layers [9]. This similarity in the system response justifies the qualitative use of the uniform damping factor for the above theoretical analysis. Nevertheless, it was shown in [9] that the different spatial distribution of the damping layers leads to differences in the shifting of the poles and zeros, so that explicitly modelling the damping layers would still be required to simulate practical terminations with higher losses. The above analysis of the multiple-wedge system may be extended to other degrees of freedom not explored here, which, apart from having more wedge terminations, may include varying the taper order [21] and using different widths or different damping for the different wedges.

4. Conclusions

A design extension to the typically used single-wedge termination of a beam has been presented in this article, where the beam is terminated by multiple quadratically tapered wedges of different lengths, which can also be arranged in a symmetric trident-shaped termination that suppresses torsion. An analytical model for the multiple-wedge termination was formulated based on the exact solutions to the non-uniform beam equation for a quadratic taper reported in [18]. A system with two wedge terminations, or three symmetrically arranged ones, was analysed. The reflection coefficient predicted by the analytical model was compared with the reflection coefficients from FE models. It was shown that, provided that the effect of torsion is effectively suppressed either by having relatively narrow beams or, more effectively, by using the trident-shaped configuration, the analytical results match well with those from FE models, albeit with discrepancies at higher frequencies. Nevertheless, the analytical model presents sufficient accuracy for a very fast method of designing and analysing the multiple-wedge termination concept over a broad frequency range and this has allowed significant insight to be made into this type of termination in this paper.

Simulations with the analytical model for different combinations of wedge lengths showed the potential for a significant decrease in the reflection coefficient, and thus absorption enhancement, compared with the single-wedge termination. Different wedge length combinations present bands of very low reflection around different frequencies. Of particular importance is the prediction of bands of nearly no reflection at low frequencies, even for relatively low damping, albeit above the lowest cut-on frequency of the individual wedges. The absorption mechanism and behaviour of the system was further investigated through an analysis of the reflection coefficient zeros in the complex-frequency plane. The analysis showed that the coupling between the wedges of different lengths introduces additional zeros to those of single-wedge terminations. For no damping, these additional zeros appear close to the real-frequency axis for wedges of similar, but different, lengths, and also for some other length combinations, and therefore require low levels of damping to achieve critical coupling and thus complete absorption. Different combinations of wedge lengths and damping will lead to different coupled modes, leading to total absorption at different frequency bands.

Overall, the introduction of the coupling between the wedges leads to an enriched modal content which in general enhances the absorptive behaviour of the system. This coupling may be further exploited by introducing periodic or

quasi-periodic arrays of wedges in a metamaterial arrangement, although this falls beyond the scope of this work. In conclusion, the presented multiple-wedge design is predicted to give significant improvement for vibration absorption compared to using a single wedge, and also opens new potential for similar design approaches within the ABH research field.

5. Acknowledgements

Angelis Karlos acknowledges support from the National Science Centre in Poland through Grant No. 2018/31/B/ST8/00753. Kristian Hook and Jordan Cheer were supported by the Intelligent Structures for Low Noise Environments (ISLNE) EPSRC Prosperity Partnership (EP/S03661X/1). Angelis Karlos would like to thank Pawel Packo for useful discussions.

Bibliography

[1] M. A. Mironov, Propagation of a flexural wave in a plate whose thickness decreases smoothly to zero in a finite interval, Soviet Physics: Acoustics 34 (3) (1988) 318–319.

[2] V. V. Krylov, New type of vibration dampers utilising the effect of acoustic 'black holes', Acta Acustica united with Acustica 90 (5) (2004) 830–837.

[3] V. V. Krylov, F. J. B. S. Tilman, Acoustic 'black holes' for flexural waves as effective vibration dampers, Journal of Sound and Vibration 274 (3-5) (2004) 605–619. doi:10.1016/j.jsv.2003.05.010.

[4] A. Pelat, F. Gautier, S. C. Conlon, F. Semperlotti, The acoustic black hole: A review of theory and applications, Journal of Sound and Vibration 476 (2020). doi:10.1016/j.jsv.2020.115316.

[5] A. Karlos, S. J. Elliott, J. Cheer, Higher-order WKB analysis of reflection from tapered elastic wedges, Journal of Sound and Vibration 449 (2019) 368–388. doi:10.1016/j.jsv.2019.02.041.

[6] L. Tang, L. Cheng, Enhanced acoustic black hole effect in beams with a modified thickness profile and extended platform, Journal of Sound and Vibration 391 (2017) 116–126. doi:10.1016/j.jsv.2016.11.010.

[7] L. Ma, H.-W. Dong, L. Cheng, An alternative and optimized thickness profile of an acoustic black hole plate, Journal of Sound and Vibration 486 (2020) 115619. doi:https://doi.org/10.1016/j.jsv.2020.115619.
URL https://www.sciencedirect.com/science/article/pii/S0022460X20304508

[8] S. Rothe, H. Watschke, S. C. Langer, Study on the producibility of additively manufactured acoustic black holes, in: 24th International Congress on Sound and Vibration, London, 2017.

[9] J. Leng, V. Romero-García, A. Pelat, R. Picó, J. P. Groby, F. Gautier, Interpretation of the acoustic black hole effect based on the concept of critical coupling, Journal of Sound and Vibration 471 (2020). doi:10.1016/j.jsv.2020.115199.

[10] J. Y. Lee, W. Jeon, Vibration damping using a spiral acoustic black hole, J. Acoust. Soc. Am. 141 (3) (2017) 1437–1445. doi:10.1121/1.4976687.

[11] J. Y. Lee, W. Jeon, Wave-based analysis of the cut-on frequency of curved acoustic black holes, Journal of Sound and Vibration 492 (2021) 115731. doi:https://doi.org/10.1016/j.jsv.2020.115731.
URL https://www.sciencedirect.com/science/article/pii/S0022460X20305617

[12] L. Zhao, Passive Vibration Control Based on Embedded Acoustic Black Holes, Journal of Vibration and Acoustics 138 (4), 041002 (05 2016). arXiv:https://asmedigitalcollection.asme.org/vibrationacoustics/article-pdf/138/4/041002/6363982/vib_138_04_041002.pdf, doi:10.1115/1.4033263.
URL https://doi.org/10.1115/1.4033263

[13] H. Li, C. Touzé, A. Pelat, F. Gautier, X. Kong, A vibro-impact acoustic black hole for passive damping of flexural beam vibrations, Journal of Sound and Vibration 450 (2019) 28–46. doi:https://doi.org/10.1016/j.jsv.2019.03.004.
URL https://www.sciencedirect.com/science/article/pii/S0022460X19301567

[14] E. P. Bowyer, D. J. O'Boy, V. V. Krylov, J. L. Horner, Effect of geometrical and material imperfections on damping flexural vibrations in plates with attached wedges of power law profile, Applied Acoustics 73 (5) (2012) 514–523. doi:10.1016/j.apacoust.2011.12.010.

[15] V. Denis, A. Pelat, F. Gautier, Scattering effects induced by imperfections on an acoustic black hole placed at a structural waveguide termination, Journal of Sound and Vibration 362 (2016) 56–71. doi:10.1016/j.jsv.2015.10.016.

[16] T. Zhou, L. Cheng, A resonant beam damper tailored with acoustic black hole features for broadband vibration reduction, Journal of Sound and Vibration 430 (2018) 174–184. doi:10.1016/j.jsv.2018.05.047.

[17] T. Zhou, L. Cheng, Planar swirl-shaped acoustic black hole absorbers for multi-directional vibration suppression, Journal of Sound and Vibration 516 (2022) 116500. doi:https://doi.org/10.1016/j.jsv.2021.116500.
URL https://www.sciencedirect.com/science/article/pii/S0022460X21005332

[18] J. Y. Lee, W. Jeon, Exact solution of Euler-Bernoulli equation for acoustic black holes via generalized hypergeometric differential equation, Journal of Sound and Vibration 452 (2019) 191–204. doi:10.1016/j.jsv.2019.02.016.

[19] L. Cremer, M. Heckl, B. A. T. Petersson, Structure-Borne Sound: Structural Vibrations and Sound Radiation at Audio Frequencies, Springer-Verlag, Germany, 2005.

[20] V. Denis, F. Gautier, A. Pelat, J. Poittevin, Measurement and modelling of the reflection coefficient of an Acoustic Black Hole termination, Journal of Sound and Vibration 349 (2015) 67–79. doi:10.1016/j.jsv.2015.03.043.

[21] K. Hook, J. Cheer, S. Daley, A parametric study of an acoustic black hole on a beam, The Journal of the Acoustical Society of America 145 (6) (2019) 3488–3498. doi:10.1121/1.5111750.

[22] J. Cheer, K. Hook, S. Daley, Active feedforward control of flexural waves in an Acoustic Black Hole terminated beam, Smart Materials and Structures 30 (3) (2021) 035003. doi:10.1088/1361-665x/abd90f.
URL https://doi.org/10.1088/1361-665x/abd90f

[23] V. Romero-García, G. Theocharis, O. Richoux, V. Pagneux, Use of complex frequency plane to design broadband and sub-wavelength absorbers, The Journal of the Acoustical Society of America 139 (6) (2016) 3395–3403. arXiv:https://doi.org/10.1121/1.4950708, doi:10.1121/1.4950708.
URL https://doi.org/10.1121/1.4950708